

# Physics-Informed Evolution: An Evolutionary Framework for Solving Quantum Control Problems Involving the Schrödinger Equation

Kaichen Ouyang<sup>\*†1</sup> and Mingyang Yu<sup>\*†2</sup>

<sup>1</sup>Department of Physics, University of Science and Technology of China, Hefei 230026, China.  
oykc@mail.ustc.edu.cn

<sup>2</sup>College of Artificial Intelligence, Nankai University, Tianjin 300350, China.  
1120240312@mail.nankai.edu.cn

\*Equal contribution. †Corresponding authors.

## Abstract

Physics-Informed Neural Networks (PINNs) have demonstrated that embedding physical laws directly into the learning objective can significantly enhance the efficiency and physical consistency of neural network solutions. Inspired by this principle, we ask a natural question: can physical information be similarly embedded into the fitness function of evolutionary algorithms? In this work, we propose **Physics-Informed Evolution (PIE)**, a novel framework that incorporates physical information derived from governing physical laws into the evolutionary fitness landscape, bridging the long-standing connection between learning and evolution in artificial intelligence. As a concrete instantiation, we apply PIE to quantum control problems governed by the Schrödinger equation, where the goal is to find optimal control fields that drive quantum systems from initial states to desired target states. We validate PIE on three representative quantum control benchmarks: state preparation in V-type three-level systems, entangled state generation in superconducting quantum circuits, and two-atom cavity QED systems, under varying levels of system uncertainty. Extensive comparisons against ten single-objective and five multi-objective evolutionary baselines demonstrate that PIE consistently achieves higher fidelity, lower state deviation, and improved robustness. Our results suggest that the physics-informed principle extends naturally beyond neural network training to the broader domain of evolutionary computation.

**Keywords:** Physics-Informed Neural Networks, Evolutionary Algorithms, Quantum Control, Schrödinger Equation, Physics-Informed Evolution, Multi-objective Optimization

# 1 Introduction

The question of how to incorporate prior knowledge about the physical world into computational optimization has long been a central concern in scientific computing and artificial intelligence. A particularly compelling recent answer comes from Physics-Informed Neural Networks (PINNs)[1], which embed physical information derived from governing physical laws directly into the neural network loss function. Rather than learning from data alone, PINNs are trained to simultaneously fit observations and satisfy the underlying physics, yielding solutions that are both accurate and physically consistent. This paradigm has proven remarkably effective across a wide range of problems in fluid mechanics, heat transfer, and inverse problems, fundamentally changing how we think about the relationship between physical models and machine learning[2].

At the same time, evolutionary computation represents a distinct and equally important tradition within artificial intelligence. Evolutionary algorithms (EAs) draw inspiration from biological evolution—selection, mutation, and reproduction—to search for optimal solutions in complex, high-dimensional, and often non-differentiable landscapes[3]. Crucially, the relationship between evolution and learning has been a recurring theme throughout the history of AI. From the Baldwin effect in evolutionary biology to the co-evolution of learning rules and population dynamics in computational models, it has long been recognized that learning and evolution are not competing paradigms but deeply intertwined processes[4, 5, 6, 7, 8]. Evolutionary algorithms have been successfully applied to a broad spectrum of optimization problems precisely because they make no assumptions about the smoothness or structure of the objective landscape, relying instead on population-level search guided by fitness evaluation.

This connection between learning and evolution naturally raises a question that, to our knowledge, has not been systematically explored: *if physical information can be embedded into the loss function of a neural network to guide learning, can it similarly be embedded into the fitness function of an evolutionary algorithm to guide evolution?* The analogy is direct. In PINNs, physical information acts as a regularizer that penalizes physically inconsistent solutions during gradient-based training. In our proposed framework, the same physical information can serve as a component of the fitness function, shaping the evolutionary landscape so that the population is guided not only toward high-performance solutions but toward solutions that respect the governing physics of the problem.

We formalize this idea as **Physics-Informed Evolution (PIE)**, a general framework in which the fitness function of an evolutionary algorithm is augmented with a physics-informed term that encodes physical information from the governing equations. PIE inherits the derivative-free, global search capability of evolutionary algorithms while gaining the physical consistency guarantees inspired by the PINN paradigm. The framework is flexible: it supports both single-objective formulations and multi-objective formulations.

As a concrete and challenging instantiation of PIE, we consider quantum control problems governed by the Schrödinger equation. Quantum control aims to find time-dependent external fields that steer a quantum system from a given initial state to a desired target state within a fixed time horizon. This is a problem of significant practical importance for quantum computing, quantum communication, and quantum information processing. We validate PIE on three representative quantum control benchmarks: state preparation in V-type three-level quantum systems, entangled state generation in superconducting quantum circuits, and control of two two-level atoms interacting with a quantized cavity field[9]. Across all three scenarios, we apply the PIE framework to multiple different single-objective and multi-objective evolutionary algorithms and analyze their performance. The results show distinct algorithm preferences across problems: adaptive differential evolution variants excel in S1 and S3 for single-objective tasks, while CMA-ES dominates S2. For multi-objective optimization, PESA2, NSGA-II, and MOEA/D each lead in different scenarios, demonstrating that algorithm selection within the PIE framework should be tailored to the specific quantum control problem.

The main contributions of this work are as follows:

- We propose Physics-Informed Evolution (PIE), a general framework that embeds physical information from governing physical laws into evolutionary fitness functions, drawing an explicit and principled analogy with the physics-informed learning paradigm.
- We develop both single-objective and multi-objective variants of PIE, enabling flexible optimization of quantum control problems under competing performance criteria, and systematically evaluate multiple evolutionary algorithms within this framework.
- We provide comprehensive empirical validation on three quantum control benchmarks with varying uncertainty levels, analyzing the performance of ten single-objective and five multi-objective evolutionary algorithms, and identifying the most effective algorithms for each specific quantum control scenario.

## 2 Related Works

### 2.1 Physics-Informed Neural Networks

The core idea of Physics-Informed Neural Networks is to embed the residual of a governing partial differential equation into the training objective of a neural network. Given a PDE of the form  $\mathcal{F}[u] = 0$  defined over a spatial-temporal domain, a PINN parameterizes the solution  $u$  as a neural network  $u_\theta$  and minimizes a composite loss:

$$\mathcal{L} = \mathcal{L}_{\text{data}} + \lambda \mathcal{L}_{\text{PDE}}, \tag{1}$$

where  $\mathcal{L}_{\text{data}}$  measures the discrepancy between the network output and available observations, and  $\mathcal{L}_{\text{PDE}} = \|\mathcal{F}[u_\theta]\|^2$  penalizes violations of the governing equation at a set of collocation points. The key insight is that the physical law acts as a form of structured regularization: it constrains the solution space to be physically consistent, enabling accurate solutions even when observational data is sparse or noisy[1].

PINNs have been applied to a wide range of forward and inverse problems, including fluid dynamics, heat conduction, wave propagation, and quantum mechanics. Extensions have addressed challenges such as imbalanced loss terms, failure modes in high-frequency or multi-scale problems, and operator learning for families of PDEs. The success of PINNs has established a broader principle: *physical laws, when expressed as differentiable residuals, can be directly incorporated into any gradient-based optimization process to guide the search toward physically meaningful solutions.*

**Bridging Learning and Evolution.** Evolutionary algorithms are population-based, derivative-free optimizers inspired by biological evolution. The relationship between learning and evolution has been foundational in AI[5], from the Baldwin effect to memetic algorithms, consistently showing these paradigms are complementary. This connection naturally extends to incorporating prior knowledge: just as physics-informed learning embeds physical laws into loss functions, the same principle transfers to evolutionary computation, where physical information shapes the fitness landscape to guide gradient-free search. The Physics-Informed Evolution framework establishes precisely this bridge between the two paradigms.

### 3 Quantum Control Problems

Quantum system control involves precisely manipulating the dynamics of a quantum system by adjusting external control fields to achieve desired quantum states or operations. Effective quantum control enhances the reliability and efficiency of quantum computation, making it crucial for quantum information processing. Multi-objective optimization algorithms can solve quantum control problems by adjusting control fields to transition a quantum system from an initial state to a target state, optimizing control functions related to field strength and timing to reach the best possible state within a given timeframe.

Key optimization objectives include fidelity, control field strength (energy consumption), and control field smoothness. In scientific research and engineering, various quantum control models target systems like atoms in multi-level structures or qubits in superconducting circuits. Despite differing physical characteristics, a quantum system’s state is generally described by a quantum state  $|\psi(t)\rangle$ , a complex vector defined by the system’s specific physical

properties. The quantum state evolution follows the Schrödinger equation (2).

$$i\hbar \frac{d}{dt} |\psi(t)\rangle = H(t) |\psi(t)\rangle \quad (2)$$

The Hamiltonian  $H(t)$  is derived from the system's energy level structure and external control fields, comprising the Hamiltonians of free, coupling, and external control fields. For a quantum system with  $M$  external control fields and  $F$  free and coupling fields as is shown in equation (3).

$$H(t) = \sum_{m=1}^M u_m(t) H_m + \sum_{f=1}^F H_f \quad (3)$$

Here,  $u_m(t)$  represents the control functions,  $H_m$  is the Hamiltonian of the control field, and  $H_f$  is the Hamiltonian of the free and coupling fields. Many quantum systems are uncertain, carrying random parameters  $\{\theta_i\}_{i=1}^{M+F}$  (fixed during control but random during each control). These parameters affect the Hamiltonian via influence functions  $\{f_i(t; \theta_i)\}_{i=1}^{M+F}$ , thereby influencing the evolution of the quantum state as in shown equation (4).

$$H(t) = \sum_{m=1}^M u_m(t) f_m(t; \theta_m) H_m + \sum_{f=1}^F f_{M+f}(t; \theta_{M+f}) H_f \quad (4)$$

The quantum system's control objective is to adjust control functions  $\{u_m(t)\}_{m=1}^M$  so that the final quantum state  $|\psi(T)\rangle$  closely matches the target state  $|\psi_{\text{target}}\rangle$  within the time  $T$ . A performance function  $J(u)$  is defined to evaluate the control strategy's quality, usually in terms of fidelity or the distance in complex space between the final and target states. The goal is to find the optimal the value of control functions that minimizes or maximizes  $|\psi(T)\rangle$ .

### 3.1 State Preparation in V-Type Three-Level Quantum Systems

A V-type three-level quantum system is a key model in quantum mechanics, consisting of three energy levels with two higher levels coupled to a common lower level. This system is crucial for understanding light-matter interactions, quantum interference, and coherence, which are essential for quantum information processing and computing. It finds applications in qubit operations, quantum gates, entangled state generation, single-photon sources, high-precision spectroscopy, and laser design, especially for multi-frequency lasers[9].

In quantum system with uncertainties, initialization, state evolution and target state of control are key steps for achieving quantum state control. As for initial state, it is usually the ground state in equation (5):

$$|\psi(0)\rangle = |g\rangle, \quad \Psi(0) = (1, 0, 0) \quad (5)$$

and the target state is typically a superposition state shown in equation (6):

$$|\psi_{\text{target}}\rangle = \frac{1}{\sqrt{2}}|e_1\rangle + \frac{1}{\sqrt{2}}|e_2\rangle, \quad \Psi_{\text{target}} = \left(0, \frac{1}{\sqrt{2}}, \frac{1}{\sqrt{2}}\right) \quad (6)$$

The evolution of the state of a quantum system is determined by the Schrödinger equation, and the key elements in Schrödinger equation is the Hamiltonian. The Hamiltonian in this problem is derived from the contribution of one free field and four external control fields as is shown in equation (7):

$$H(t) = f_0(t; \theta_0)H_0 + \sum_{m=1}^4 u_m(t)f_m(t; \theta_m)H_m \quad (7)$$

Where  $H_0$  is the free Hamiltonian, and the control Hamiltonians are  $H_i, i = 1, 2, 3, 4$ . The formula of them are shown in equation (8).

$$\begin{aligned} H_0 &= \begin{pmatrix} 1.5 & 0 & 0 \\ 0 & 1 & 0 \\ 0 & 0 & 1 \end{pmatrix}, H_1 = \begin{pmatrix} 0 & 1 & 0 \\ 1 & 0 & 0 \\ 0 & 0 & 0 \end{pmatrix}, H_2 = \begin{pmatrix} 0 & -i & 0 \\ i & 0 & 0 \\ 0 & 0 & 0 \end{pmatrix}, \\ H_3 &= \begin{pmatrix} 0 & 0 & 1 \\ 0 & 0 & 0 \\ 1 & 0 & 0 \end{pmatrix}, H_4 = \begin{pmatrix} 0 & 0 & -i \\ 0 & 0 & 0 \\ i & 0 & 0 \end{pmatrix} \end{aligned} \quad (8)$$

These are designed based on quantum control theory, Lie algebras, and the Lyapunov control method, starting from the generators of the  $SU(3)$  group. The influence function for the uncertainty parameters is given by  $f_0(t; \theta_0) = 1 - \epsilon\theta \cos t$ ,  $f_i(t; \theta_i) = 1$ ,  $i = 1, 2, 3, 4$ , where  $\epsilon$  is an inherent parameter of the quantum system.

## 3.2 Superconducting Quantum Circuits

Superconducting quantum circuits, based on Josephson junctions, demonstrate quantum behavior similar to artificial atoms, making them vital for quantum computing and quantum information processing. Their flexibility and scalability enable the construction of qubits, the fundamental units of quantum computing, with the potential for large-scale integration due to long coherence times and high operational precision. These circuits are key in validating fundamental principles of quantum mechanics, crucial for both applied and fundamental research[9].

In superconducting quantum circuits, two primary types of qubits—flux qubits and charge qubits—are controlled by adjusting external parameters like magnetic flux  $\Phi$  and gate voltage

$V_g$ . The basic Hamiltonian for charge qubits is given by equation (9).

$$H = F_z(V_g)\sigma_z - F_x(\Phi)\sigma_x \quad (9)$$

Here  $F_z(V_g)\sigma_z$  and  $F_x(\Phi)\sigma_x$  are respectively related to the charging energy  $E_C$  and  $E_J$ , which can be adjusted by external parameters such as the voltage  $V_g$  and the magnetic flux  $\Phi$ . Meanwhile  $\sigma_z$  and  $\sigma_x$  are Pauli matrices.

In more complex operations, coupled two-qubit systems use an LC oscillator, leading to a Hamiltonian of the form in equation (10):

$$H = \sum_{i=1}^2 [F_z(V_i)\sigma_z(i) + F_x(\Phi_i)\sigma_x(i)] + \chi(\gamma)\sigma_z(1) \otimes I(2) \quad (10)$$

After normalization and simplification, the expression of Hamiltonian is shown in equation (11):

$$\begin{aligned} \frac{H}{\hbar} = & \theta_1 u_1(t) \sigma_z(1) \otimes I(2) + \theta_2 u_2(t) \sigma_z(1) \otimes \sigma_z(2) - \theta_3 u_3(t) \sigma_x(1) \otimes I(2) \\ & - \theta_4 u_4(t) \sigma_x(1) \otimes \sigma_z(2) - \theta_5 u_5(t) \sigma_y(1) \otimes \sigma_y(2) \end{aligned} \quad (11)$$

In the normalized Hamiltonian formula,  $\theta_m$  represents coefficients of uncertainty parameters with specific values varying within a given range, while  $u_i(t)$  are control functions used to manipulate the state of the qubits. This formulation expresses the system's Hamiltonian in a simplified form that includes uncertainty and control parameters, facilitating more convenient control and optimization in practical operations. Where  $\theta_m$  represents uncertainty coefficients, and  $u_i(t)$  are control functions that manipulate the qubits' states.

The initial state of control is the ground state as is shown in equation (12).

$$|\psi(0)\rangle = |g_1 g_2\rangle, \quad \Psi(0) = (1, 0, 0, 0) \quad (12)$$

and the target state of control is the maximally entangled state as is shown in equation (13).

$$|\psi_{\text{target}}\rangle = \frac{1}{\sqrt{2}}(|g_1 e_2\rangle + |e_1 g_2\rangle), \quad \Psi_{\text{target}} = \left(0, \frac{1}{\sqrt{2}}, \frac{1}{\sqrt{2}}, 0\right) \quad (13)$$

### 3.3 A quantum system consisting of two two-level atoms

The quantum system of two two-level atoms interacting with a quantized field in a cavity is widely used in experimental quantum optics and information processing, offering key insights into entangled state dynamics. Controlling entanglement between atoms is vital for quantum

communication and computation, enabling tasks like teleportation, key distribution, and gate operations. Effective control ensures high-fidelity generation and manipulation of entangled states, essential for robust quantum computing and secure communication[9].

The Hamiltonian governing the dynamics of this system comprises contributions from the free evolution of the atoms and the field, the interaction between the atoms, and the interaction between the atoms and the field. It is expressed as equation (14).

$$H(t) = H_0 + H_I + H_u \quad (14)$$

where:

$H_0$  represents the energy of the atoms and the field,

$H_I$  denotes the interaction between the atoms and the interaction between the atoms and the field,

$H_u$  is the control Hamiltonian, which allows for the manipulation of the system's state through external controls.

The specific forms of these Hamiltonians are in equation (15), (16) and (17).

$$H_0 = \frac{1}{2} \sum_{i=1}^2 \omega_{A_i} \sigma_z^{(i)} + \omega_r a^\dagger a, \quad (15)$$

$$H_I = \sum_{i \neq j} \Omega_{ij} \sigma_+^{(i)} \otimes \sigma_-^{(j)} + \sum_j v_j \left( a^\dagger \sigma_-^{(j)} + a \sigma_+^{(j)} \right), \quad (16)$$

$$H_u = \sum_{i=1}^2 u_{\omega_{A_i}}(t) \sigma_z^{(i)} + u_{\omega_r}(t) a^\dagger a + \sum_{i \neq j} u_{\Omega_{ij}}(t) \sigma_+^{(i)} \otimes \sigma_-^{(j)} + \sum_j u_{v_j}(t) \left( a^\dagger \sigma_-^{(j)} + a \sigma_+^{(j)} \right). \quad (17)$$

Here,  $\omega_{A_i}$  and  $\omega_r$  are the atomic transition frequencies and the field frequency, respectively;  $\Omega_{ij}$  is the dipole-dipole interaction parameter; and  $v_j$  is the coupling constant between the atoms and the quantized field. The control problem involves driving the system from an initial ground state as is shown in equation (18).

$$|\psi(0)\rangle = |g_1 g_2\rangle, \quad \Psi(0) = (1, 0, 0, 0) \quad (18)$$

where both atoms are in their ground states, to a target maximally entangled state as is shown in equation (19).

$$|\psi_{\text{target}}\rangle = \frac{1}{\sqrt{2}}(|g_1 e_2\rangle + |e_1 g_2\rangle), \quad \Psi_{\text{target}} = \left( 0, \frac{1}{\sqrt{2}}, \frac{1}{\sqrt{2}}, 0 \right) \quad (19)$$

## 4 Physics-Informed Evolution

### 4.1 Search Space Encoding and State Evolution

The control functions  $u$  of the quantum system are the variables solved by the optimization algorithm, mapped to the algorithm's search space through grid sampling. We uniformly take  $N$  sample points, corresponding to times  $\{t_0, t_1, \dots, t_N\} = \{0, \frac{T}{N}, \frac{2T}{N}, \dots, \frac{(N-1)T}{N}, T\}$ , where  $T$  is the total control time. The values of each control function at the first  $N$  points form the search space of the optimization algorithm. If there are  $M$  control functions, the search space has  $M \times N$  dimensions, meaning a particle in the optimization algorithm is in equation (20).

$$Pos(i) = \{u_1(t_0), u_1(t_1), \dots, u_1(t_{N-1}), u_2(t_0), u_2(t_1), \dots, u_2(t_{N-1}), \dots, u_M(t_0), u_M(t_1), \dots, u_M(t_{N-1})\} \quad (20)$$

Given the value of control functions and uncertain parameters, we can use the finite difference method to solve the Schrödinger equation and calculate the system's state  $\Psi$  of the system at these sample points; that is, for the Schrödinger equation like (21).

$$i\hbar \frac{d}{dt} |\psi(t)\rangle = H(t) |\psi(t)\rangle = \left( \sum_{i=1}^M u_i(t) f_i(t; \theta_i) H_i(t) + \sum_{j=M+1}^{M+F} f_j(t; \theta_j) H_j(t) \right) |\psi(t)\rangle \quad (21)$$

Here, in equation (21),  $\{u_i(t)\}_{i=1}^M$  are the control functions,  $\{f_i(t; \theta_i)\}_{i=1}^{M+F}$  are the influence functions of the uncertain parameters, and  $\{H_i(t)\}_{i=1}^{M+F}$  are the Hamiltonians. Using the finite difference method for numerical calculations, the states  $\{\Psi(t_i)\}_{i=0}^N$  at the sample points follow the recursion formula (22).

$$\Psi(t_{i+1}) = \Psi(t_i) + \frac{d}{dt} \Psi(t_i) \Delta t = \Psi(t_i) - \frac{i}{\hbar} H(t_i) \Psi(t_i) \Delta t \quad (22)$$

This allows us to calculate the state  $\{\Psi(t_i)\}_{i=0}^N$  of the system over the entire control time  $T$ .

If the sample points are too few, the finite difference method's numerical error increases; too many points, and the optimization algorithm's search space becomes too large. To address this, we use spline interpolation. Assuming the number of sample points in the search space is  $N$ , we interpolate the value of control functions  $\{u_i(t_j)\}_{j=0}^{N-1}$  to  $\{u_i(t_j)\}_{j=0}^{\alpha(N-1)}$ , where  $\alpha$  is our interpolation factor, and  $\{t_j\}_{j=0}^{\alpha(N-1)}$  are the uniformly sampled points by taking  $\alpha N$  as the sampling number. This ensures numerical accuracy while keeping the search space manageable.

## 4.2 Single-objective Physics-informed Evolution

**Performance Function.** The primary optimization objective is the performance function  $J(u)$ , usually defined as fidelity, which is based on the final state  $\Psi(T)$  of the quantum system and the target state  $\Psi_{\text{target}}$ . We aim to maximize this fidelity, typically calculated as the square of the modulus of the inner product of these two states for pure quantum states as is shown in equation (23).

$$J(u) = \text{Fidelity} = |\langle \Psi(T) | \Psi_{\text{target}} \rangle|^2 \quad (23)$$

For mixed quantum states, it is the trace distance between the two states. First, we calculate the density matrices  $\rho(T)$  and  $\rho_{\text{target}}$  of the two states as is shown in equation (24).

$$\rho(T) = |\Psi(T)\rangle\langle\Psi(T)|, \quad \rho_{\text{target}} = |\Psi_{\text{target}}\rangle\langle\Psi_{\text{target}}| \quad (24)$$

then calculate the trace distance between the two density matrices as is shown in equation (25).

$$J(u) = \text{Fidelity} = \text{Tr} \left( \sqrt{\sqrt{\rho(T)}\rho_{\text{target}}\sqrt{\rho(T)}} \right) \quad (25)$$

In the three quantum control problems mentioned, the first two involve pure states, while the third involves a mixed state. Fidelity, defined by the alignment of vectors in complex space, is maximized when the final state and target state are aligned or opposite. However, this can lead to optimization challenges, as optimal solutions may cluster in two distant areas of the search space, complicating convergence. To address this, we use the distance deviation between quantum states as the optimization objective instead of fidelity, measuring performance by the distance in complex space, as is shown in equation (26).

$$J(u) = \text{Deviation} = \|\Psi(T) - \Psi_{\text{target}}\| \quad (26)$$

For mixed quantum states, as is shown in equation (27).

$$J(u) = \text{Deviation} = \|\rho(T) - \rho_{\text{target}}\| \quad (27)$$

Our optimization goal is to minimize or maximize Deviation, which we refer to as positive fidelity optimization and negative fidelity optimization, respectively.

**Energy Consumption.** In quantum control optimization, besides maximizing fidelity, energy consumption, which reflects the cost of control, must also be considered. We define

the energy consumption objective function as the equation (28).

$$\text{Energy} = \sum_{i=1}^M \int_0^T |u_i(t)| \cdot \|H_i(t)\| dt = \sum_{i=1}^M \sum_{j=1}^N |u_i(t_j)| \cdot \|H_i(t_j)\| \cdot \Delta t \quad (28)$$

Where  $M$  is the number of control fields,  $N$  is the number of sample points in the numerical calculation, and  $\Delta t = \frac{T}{N}$  is the time interval between sample points.

**Overall Fitness Function.** Drawing inspiration from Physics-Informed Neural Networks (PINNs), where the loss function combines a data fidelity term and a physics-informed regularization term, we similarly construct the fitness function for Physics-Informed Evolution. In this framework, the state deviation term Deviation serves as the analog of the *data loss* in PINNs—it measures how well the control strategy achieves the desired target state. The energy consumption term Energy acts as the analog of the *physics-informed regularization*—it encodes physical prior knowledge about the control cost and guides the search toward physically meaningful and efficient solutions. This energy term implicitly reflects the physical principle that control fields should be as weak as possible while still achieving the control objective, analogous to the principle of least action in physics. By combining these two terms, we define the overall fitness function as a weighted sum:

$$F(u) = \text{Deviation} + \lambda \cdot \text{Energy} \quad (29)$$

where  $\lambda$  is a regularization parameter that balances the trade-off between minimizing the state deviation (task performance) and minimizing the energy consumption (physical cost). A smaller  $\lambda$  places more emphasis on achieving high-fidelity state preparation, while a larger  $\lambda$  prioritizes energy-efficient control strategies that respect the physical constraints of the system. The optimization goal is to minimize  $F(u)$ , thereby seeking control solutions that are both accurate and physically consistent.

### 4.3 Multi-objective Physics-informed Evolution

While the single-objective formulation combines state deviation and energy consumption into a weighted sum, this approach requires tuning the regularization parameter  $\lambda$  and assumes a fixed preference between the two objectives. In many quantum control problems, however, the trade-off between fidelity and energy efficiency is not known a priori, motivating a multi-objective formulation.

In the multi-objective PIE framework, we treat Deviation and Energy as two separate objectives to be minimized simultaneously:

$$\underset{u}{\text{minimize}} \quad \mathbf{F}(u) = (\text{Deviation}(u), \text{Energy}(u)) \quad (30)$$

Following the same physics-informed philosophy, Deviation measures task performance (how accurately the target state is achieved), while Energy encodes the physical cost of control. Rather than seeking a single optimal solution, we seek a set of Pareto-optimal solutions representing different trade-offs between these two competing objectives. A control strategy  $u_a$  dominates  $u_b$  if it performs no worse on both objectives and strictly better on at least one. The set of non-dominated solutions forms the Pareto front, providing decision-makers with a range of physically feasible control strategies—from high-fidelity but energy-intensive to energy-efficient but slightly lower fidelity. This multi-objective formulation eliminates the need for parameter tuning and offers richer decision support for quantum control tasks.

## 5 Experimental Results and Analysis

### 5.1 Experimental Setup

To thoroughly evaluate the proposed method and ensure representative comparisons, we adopt a set of widely used evolutionary optimizers as baselines. The single-objective algorithms include Differential Evolution (DE)[10], Evolution Strategy with Covariance Matrix Adaptation (CMA-ES)[11], Mixture Model-Based Evolution Strategy (MMES)[12], Evolution Strategy Based on Search Direction Adaptation (SDAES)[13], Self-adaptive Differential Evolution (SaDE)[14], Adaptive Differential Evolution with Optional External Archive (JADE)[15], Chaotic Local Search-based Differential Evolution (CJADE)[16], Success-History Based Parameter Adaptation for Differential Evolution (SHADE)[17], Improving the Search Performance of SHADE Using Linear Population Size Reduction (LSHADE)[18], and Four Evolutionary Algorithms with Eigen crossover (EA4eig)[19], whereas the multiobjective algorithms include Nondominated Sorting Genetic Algorithm II (NSGA-II)[20], Reference-point-based Many Objective Evolutionary Algorithm Following NSGA-II Framework (NSGA-III)[21], A Multiobjective Evolutionary Algorithm Based on Decomposition (MOEA/D)[22], Strength Pareto Evolutionary Algorithm 2 (SPEA2)[23], and Modified Pareto Envelop-based Selection Algorithm (PESA2)[24, 25]. These baselines cover differential evolution (and its adaptive variants), evolution strategies, and mainstream multiobjective evolutionary frameworks.

For a fair comparison, all algorithms are run under the same computational budget with population size  $N = 50$  and maximum iterations  $T = 500$ , and each algorithm is independently executed 30 times. The algorithm parameters all follow the regulations in Table I and the implementation method in the original paper to avoid deviations caused by parameter adjustments. Experiments are conducted on an Intel Core i5-12400 CPU (2.50 GHz) with 16 GB RAM, using MATLAB R2023a.

Table 1: Parameter configurations for competing algorithms

Algorithms	Specific parameters
DE	$F = 0.5, CR = 0.5$
CMA-ES	$\lambda = 4 + \lfloor 3 \ln n \rfloor, \mu = \lfloor \lambda/2 \rfloor, \omega_i = \frac{\ln(\mu+0.5) - \ln(i)}{\mu \ln(\mu+0.5) - \sum_{j=1}^{\mu} \ln(j)}, \mu_{eff} = \frac{1}{\sum_{i=1}^{\mu} \omega_i^2}, c_c = 0.4/\sqrt{n}$
MMES	$\lambda = 4 + \lfloor 3 \ln n \rfloor, \mu = \lfloor \lambda/2 \rfloor, m = 2 \lceil \sqrt{n} \rceil, c_a = 4/n, c_c = 0.4/\sqrt{n}, T = \lceil 1/c_c \rceil, \gamma = 1 - (1 - c_a)^m, \omega_i = \frac{\ln(\mu+0.5) - \ln(i)}{\mu \ln(\mu+0.5) - \sum_{j=1}^{\mu} \ln(j)}, \mu_{eff} = \frac{1}{\sum_{i=1}^{\mu} \omega_i^2}, c_{\sigma} = 0.3, d_{\sigma} = 1, \alpha_z = 0.05$
SDAES	$\lambda = 4 + \lfloor 3 \ln n \rfloor, \mu = \lfloor \lambda/2 \rfloor, m = 10, c_{cov} = 0.4/\sqrt{n}, c_c = 0.25/\sqrt{n}, \omega_i = \frac{\ln(\mu+1) - \ln(i)}{\mu \ln(\mu+1) - \sum_{j=1}^{\mu} \ln(j)}, \mu_{eff} = \frac{1}{\sum_{i=1}^{\mu} \omega_i^2}, c_s = 0.3, d_{\sigma} = 1, p^* = 0.05$
SaDE	$LP = 50, CR = \text{adaptive}$
JADE	$p = [0.05, 0.2], c = [0.05, 0.2], \mu_{CR} = 0.5, \mu_{CF} = 0.5$
CJADE	$Radius = 0.001, c = 0.1, p = 0.05, CRm = 0.5, Fm = 0.5, A_{factor} = 1$
SHADE	$NP = 50, H = [30, 100]$
LSHADE	$NP_{init} = 50, NP_{min} = 4, p = 0.11,  A  = 2.6, H = 6$
EA4eig	$NP_{init} = 50, NP_{min} = 10, p_{best\_rate} = 0.11,  A  = 2.6, H = 4$
NSGA-II	$NP = 50, p_c = 0.9, p_m = 1/D, \eta_c = 20, \eta_m = 20$
NSGA-III	$NP \approx H, p_c = 0.9, p_m = 1/D, \eta_c = 30, \eta_m = 20$
MOEA/D	$NP = 50, T = 20, \delta = 0.9, n_r = 2$
SPEA2	$NP = 50, \text{Archive} = 50, p_c = 0.9, p_m = 1/D$
PESA2	$NP = 50, \text{Archive} = 50, \text{Grid} = 32, p_c = 0.9, p_m = 1/D$

## 5.2 Experiments on Single-objective Physics-informed Evolution

We evaluate the single-objective PIE framework by comparing ten evolutionary algorithms across three quantum control scenarios (S1, S2, S3) under five different regularization parameter settings ( $\lambda = 0, 0.1, 0.01, 0.001, 0.0001$ ). Table 2 reports the mean and standard deviation of Fidelity, Deviation, Energy, and RunTime for each algorithm over 30 independent runs. The regularization parameter  $\lambda$  in the fitness function  $F(u) = \text{Deviation} + \lambda \cdot \text{Energy}$  controls the trade-off between state accuracy and energy efficiency: smaller  $\lambda$  emphasizes minimizing state deviation, while larger  $\lambda$  prioritizes energy-efficient control.

Figure 1 illustrates the experimental results of quantum control in the single-objective Physics-informed Evolution framework across the three problems. It visualizes the evolution of the physical field  $u$  and the quantum state  $\psi$ , demonstrating the dynamic behavior of the control inputs and the corresponding state responses throughout the optimization process.

**Performance under Pure State Deviation Optimization ( $\lambda = 0$ ).** When energy consumption is completely disregarded ( $\lambda = 0$ ), most algorithms achieve near-perfect fidelity

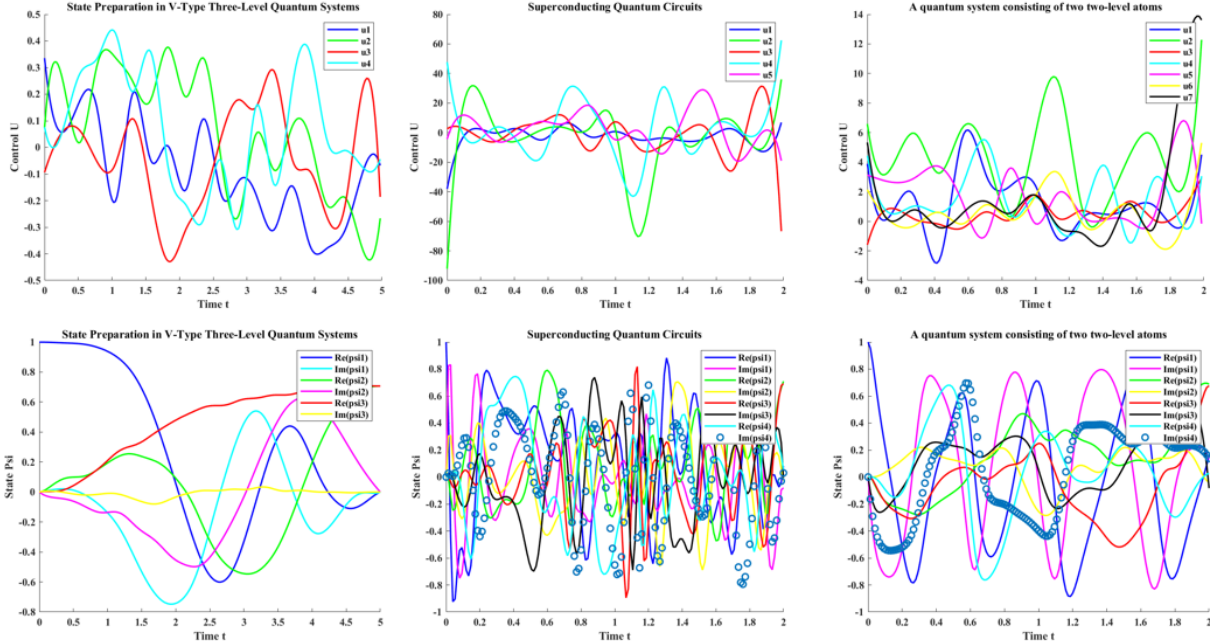


Figure 1: Evolution of control inputs  $u$  and quantum state  $\psi$  for three quantum control problems (S1, S2, S3) in the Single-Objective Physics-informed Evolution framework.

across all scenarios. SaDE demonstrates exceptional performance in S1, achieving the lowest deviation ( $8.65 \times 10^{-17}$ ) while maintaining relatively low energy consumption (3.87). CMA-ES excels in S2, achieving perfect fidelity (1.00) and the lowest deviation ( $1.59 \times 10^{-5}$ ). For S3, CJADE achieves the highest fidelity ( $9.99 \times 10^{-1}$ ) while CMA-ES again obtains the lowest deviation ( $4.17 \times 10^{-4}$ ). Regarding energy efficiency, EA4eig consistently achieves the lowest energy consumption across all three scenarios (3.32, 2.82, and  $1.05 \times 10^2$  respectively), albeit with slightly lower fidelity in some cases, demonstrating its inherent bias toward energy-efficient solutions even when not explicitly weighted. MMES and SDAES exhibit the shortest runtimes, typically around 32 – 34 seconds, making them suitable for time-sensitive applications.

**Performance with Strong Energy Regularization ( $\lambda = 0.1$ ).** When energy consumption is given substantial weight, performance patterns shift notably. In S1, DE achieves the highest fidelity ( $9.20 \times 10^{-1}$ ) and lowest deviation ( $2.06 \times 10^{-2}$ ), suggesting its robustness to the regularization term. For S2, MMES shows superior performance with fidelity  $9.38 \times 10^{-1}$  and deviation  $1.92 \times 10^{-2}$ , outperforming all other algorithms under this regularization strength. In S3, SDAES achieves the best results with fidelity  $8.63 \times 10^{-1}$  and deviation  $8.15 \times 10^{-2}$ . Energy consumption at this  $\lambda$  value reveals which algorithms best balance the trade-off: SHADE achieves the lowest energy in S1 (2.01) and S3 (3.64), while EA4eig remains most energy-efficient in S2 (2.11). Runtime leaders are EA4eig for S1 (59.2), SDAES for S2 (46.0) and S3 (66.5), showing that simpler algorithms often converge faster

under stronger regularization.

**Performance with Moderate Energy Regularization ( $\lambda = 0.01$  and  $0.001$ ).** As the regularization parameter decreases, the emphasis shifts back toward state accuracy. At  $\lambda = 0.01$ , CMA-ES leads in S1 fidelity ( $9.99 \times 10^{-1}$ ), while JADE achieves the lowest deviation ( $2.27 \times 10^{-4}$ ). For S2, CMA-ES again dominates with perfect fidelity and deviation  $3.17 \times 10^{-4}$ . In S3, SDAES achieves the highest fidelity ( $9.85 \times 10^{-1}$ ) and lowest deviation ( $9.94 \times 10^{-3}$ ). At  $\lambda = 0.001$ , adaptive algorithms show remarkable performance: JADE, CJADE, and SHADE all achieve perfect fidelity in S1, with CJADE attaining the lowest deviation ( $3.32 \times 10^{-6}$ ). CMA-ES maintains dominance in S2 with fidelity 1.00 and deviation  $1.37 \times 10^{-4}$ . For S3, CJADE again leads with fidelity  $9.93 \times 10^{-1}$  and deviation  $3.35 \times 10^{-3}$ . Energy consumption at these regularization levels shows SHADE and CJADE as consistently efficient, while runtime advantages persist for MMES and SDAES.

**Performance with Weak Energy Regularization ( $\lambda = 0.0001$ ).** At the smallest regularization strength, algorithms focus almost exclusively on state accuracy. In S1, SaDE, JADE, CJADE, and SHADE all achieve near-perfect fidelity (1.00), with SaDE obtaining the lowest deviation ( $1.91 \times 10^{-7}$ ). CMA-ES continues to excel in S2 with fidelity  $9.99 \times 10^{-1}$  and deviation  $1.62 \times 10^{-4}$ . For S3, CJADE maintains its leadership with fidelity  $9.98 \times 10^{-1}$  and deviation  $7.91 \times 10^{-4}$ . SHADE achieves the lowest energy in S1 (3.11) and S3 ( $1.04 \times 10^2$ ), while EA4eig remains most energy-efficient in S2 (2.62). SDAES consistently provides the fastest runtime across all scenarios.

**Overall Observations.** Several patterns emerge from the comprehensive comparison across different regularization strengths. First, adaptive differential evolution variants (JADE, CJADE, SHADE) consistently achieve the highest fidelity and lowest deviation, particularly as  $\lambda$  decreases, demonstrating their effectiveness in prioritizing state accuracy within the PIE framework. Second, CMA-ES shows remarkable performance in S2 across all  $\lambda$  values, suggesting its suitability for specific quantum control landscapes regardless of regularization strength. Third, EA4eig consistently achieves the lowest energy consumption in S2, indicating its inherent strength in finding energy-efficient solutions even when the regularization term is small. Fourth, MMES and SDAES consistently provide the shortest runtimes, making them practical choices when computational efficiency is paramount. Finally, the trade-off controlled by  $\lambda$  is clearly visible: as  $\lambda$  increases, energy consumption generally decreases, but at the cost of higher state deviation. Different algorithms navigate this trade-off with varying degrees of success depending on the scenario and the specific  $\lambda$  value, validating the PIE framework’s ability to generate a spectrum of solutions from high-fidelity to energy-efficient control strategies.

Table 2: Single-objective

$\lambda$	Scene	Metrics (Mean±Std)	DE	CMA ES	MMES	SDAES	SAde	JAde	CJAde	SHADE	LSHADE	EA4eig	
0	S1	Fidelity	9.99E-01±4.54E-04	1.00E+00±3.65E-05	9.99E-01±4.49E-03	1.00E+00±1.90E-07	<b>1.00E+00±4.93E-16</b>	1.00E+00±2.86E-08	1.00E+00±6.11E-08	1.00E+00±2.37E-08	1.00E+00±1.53E-05	9.67E-01±1.79E-01	
		Deviation	2.77E-04±1.14E-04	1.97E-05±1.15E-05	3.11E-04±1.13E-03	8.91E-09±4.88E-08	<b>8.65E-17±4.49E-16</b>	1.12E-08±8.05E-09	1.30E-08±1.99E-08	3.47E-09±6.74E-09	1.03E-05±4.75E-06	1.47E-02±8.00E-02	
		Energy	5.64E+00±2.55E-01	1.80E+01±3.68E+00	1.06E+03±9.74E+01	1.14E+03±1.53E+02	3.87E+00±2.56E-01	3.73E+00±1.76E-01	4.14E+00±2.62E-01	3.84E+00±1.92E-01	4.54E+00±2.68E-01	<b>3.32E+00±4.37E-01</b>	4.69E+01±4.40E+00
	S2	RunTime	9.25E+01±2.85E+00	1.24E+02±5.25E+00	3.26E+01±1.39E+00	<b>3.23E+01±1.90E+00</b>	9.69E+01±3.86E+00	1.92E+02±5.08E+00	9.77E+01±3.44E+00	9.70E+01±2.87E+00	9.58E+01±3.41E+00	4.69E+01±4.40E+00	
		Fidelity	9.12E-01±4.07E-03	<b>1.00E+00±3.60E-05</b>	9.98E-01±6.10E-03	1.00E+00±2.25E-04	9.05E-01±2.02E-02	8.87E-01±3.20E-02	9.14E-01±3.34E-03	9.14E-01±3.34E-03	9.10E-01±1.69E-02	5.13E-01±2.12E-01	
		Deviation	2.48E-02±1.12E-03	<b>1.59E-05±9.38E-06</b>	4.03E-04±1.54E-03	3.04E-05±5.65E-05	2.69E-02±5.39E-03	3.24E-02±8.68E-03	2.43E-02±9.21E-04	2.41E-02±8.75E-04	1.56E-02±4.24E-03	1.99E-01±1.06E-01	
	S3	Energy	4.67E+00±6.39E-02	1.11E+01±1.16E+00	5.19E+02±4.03E+01	5.47E+02±7.46E+01	4.70E+00±4.44E-02	4.34E+00±7.94E-02	4.76E+00±1.45E-02	4.76E+00±8.19E-03	4.76E+00±2.72E-02	<b>2.82E+00±5.11E-01</b>	
		RunTime	9.63E+01±2.59E+00	1.31E+02±5.26E+00	3.32E+01±1.79E+00	<b>3.30E+01±2.07E+00</b>	1.04E+02±4.61E+00	2.08E+02±6.05E+00	1.06E+02±4.50E+00	1.06E+02±4.46E+00	1.04E+02±5.10E+00	4.85E+01±7.23E+00	
		Fidelity	9.94E-01±2.91E-03	9.99E-01±1.03E-03	9.73E-01±5.51E-02	9.83E-01±5.77E-02	9.98E-01±1.48E-03	9.99E-01±1.61E-03	<b>9.99E-01±7.73E-04</b>	9.99E-01±8.62E-04	9.97E-01±2.91E-03	9.18E-01±5.44E-02	
	0.1	S1	Deviation	3.45E-03±1.71E-03	<b>4.17E-04±5.08E-04</b>	1.33E-02±2.76E-02	8.56E-03±2.93E-02	9.87E-04±8.57E-04	7.57E-04±8.02E-04	4.93E-04±3.92E-04	5.58E-04±4.34E-04	1.54E-03±1.55E-03	6.17E-01±3.01E-01
			Energy	1.37E+02±1.17E+01	4.49E+02±9.59E+01	1.08E+03±1.48E+02	1.15E+03±1.74E+02	1.41E+02±1.09E+01	1.14E+02±7.85E+00	1.18E+02±1.05E+01	1.17E+02±1.01E+01	1.27E+02±1.18E+01	<b>1.05E+02±3.39E+00</b>
			RunTime	1.03E+02±4.75E+00	1.32E+02±1.70E-01	3.40E+01±2.78E-01	<b>3.40E+01±9.60E-02</b>	1.01E+02±4.85E-01	2.01E+02±9.52E-01	1.02E+02±3.65E-01	1.01E+02±5.53E-01	1.01E+02±4.84E-01	4.87E+01±1.97E+00
S2		Fidelity	<b>9.20E-01±1.69E-02</b>	9.16E-01±4.45E-03	7.92E-01±2.54E-01	9.07E-01±1.37E-01	9.14E-01±4.26E-03	9.16E-01±4.05E-03	9.16E-01±3.23E-03	9.17E-01±3.10E-03	9.17E-01±2.71E-03	8.80E-01±1.65E-01	
		Deviation	<b>2.06E-02±4.43E-03</b>	2.17E-02±1.09E-03	6.84E-02±8.58E-02	2.93E-02±4.05E-02	2.21E-02±1.14E-03	2.17E-02±9.72E-04	2.19E-02±9.03E-04	2.21E-02±9.19E-04	2.15E-02±8.18E-04	4.05E-02±9.53E-02	
		Energy	2.23E+00±4.41E-02	2.05E+00±8.80E-03	2.57E+01±1.18E+01	1.90E+01±6.12E+00	2.06E+00±1.35E-02	2.02E+00±9.60E-03	2.02E+00±1.32E-02	<b>2.01E+00±1.39E-02</b>	2.02E+00±1.14E-02	2.44E+00±2.27E-01	
S3		RunTime	1.15E+03±5.46E+03	1.76E+02±5.29E+01	7.15E+01±2.09E+00	7.09E+01±2.25E+00	2.15E+02±2.06E+00	2.59E+02±4.93E+01	1.74E+02±4.22E+01	1.24E+02±2.54E+00	1.24E+02±3.32E-01	<b>5.92E+01±2.28E+00</b>	
		Fidelity	7.72E-01±1.57E-02	9.15E-01±2.14E-03	<b>9.38E-01±3.25E-02</b>	8.53E-01±1.91E-01	6.59E-01±2.63E-01	7.16E-01±1.49E-01	7.04E-01±1.66E-01	7.06E-01±1.92E-01	7.57E-01±6.72E-03	3.67E-01±2.40E-01	
		Deviation	7.92E-02±5.15E-03	3.23E-02±7.79E-04	<b>1.92E-02±8.97E-03</b>	5.16E-02±8.96E-02	1.39E-01±1.44E-01	1.04E-01±7.74E-02	1.06E-01±8.01E-02	1.12E-01±1.06E-01	8.40E-02±1.82E-03	2.86E-01±1.40E-01	
0.01		S1	Energy	3.02E+00±7.40E-02	3.17E+00±8.15E-03	1.93E+01±8.14E+00	1.13E+01±3.98E+00	2.52E+00±1.00E+00	2.78E+00±5.32E-01	2.75E+00±5.35E-01	2.69E+00±7.31E-01	2.89E+00±1.87E-02	<b>2.11E+00±7.37E-01</b>
			RunTime	1.79E+02±4.59E+01	2.62E+02±2.32E+01	4.75E+01±1.21E+00	<b>4.60E+01±4.81E-01</b>	1.42E+02±5.22E-01	2.85E+02±7.02E-01	1.53E+02±3.18E+00	1.49E+02±2.76E-01	1.48E+02±2.62E-01	6.53E+01±1.28E+01
			Fidelity	7.87E-01±7.59E-02	8.16E-01±1.69E-02	8.16E-01±1.51E-01	<b>8.63E-01±8.96E-02</b>	7.70E-01±3.77E-02	7.62E-01±3.05E-02	7.57E-01±2.86E-02	7.60E-01±2.98E-02	7.67E-01±2.68E-02	5.66E-01±1.98E-01
	S2	Deviation	1.32E-01±5.22E-02	9.23E-02±8.57E-03	9.98E-02±8.07E-02	<b>8.15E-02±5.13E-02</b>	1.25E-01±2.24E-02	1.26E-01±1.86E-02	1.27E-01±1.70E-02	1.24E-01±1.73E-02	1.23E-01±1.50E-02	5.14E-01±1.99E-01	
		Energy	2.39E+01±8.64E-01	3.65E+00±2.98E-01	4.97E+01±1.41E+01	3.37E+01±8.69E+00	1.09E+01±1.45E+00	5.11E+00±3.03E+00	4.06E+00±2.40E+00	<b>3.64E+00±1.88E+00</b>	3.86E+00±1.27E+00	4.97E+00±2.32E+01	
		RunTime	2.07E+02±7.16E+00	2.56E+02±1.51E+02	6.92E+01±1.64E+00	6.65E+01±1.75E-01	1.95E+02±3.51E-01	3.90E+02±5.01E+00	1.98E+02±3.37E-01	1.97E+02±3.31E-01	1.95E+02±3.16E-01	7.94E+01±1.73E+01	
	S3	Fidelity	9.95E-01±2.82E-03	<b>9.99E-01±1.49E-04</b>	8.75E-01±1.86E-01	9.27E-01±1.21E-01	9.99E-01±1.64E-04	9.99E-01±7.05E-05	9.99E-01±7.20E-05	9.99E-01±6.93E-05	9.99E-01±9.27E-05	9.66E-01±1.81E-01	
		Deviation	1.65E-03±7.75E-04	2.32E-04±3.64E-05	4.07E-02±6.19E-02	2.07E-02±3.48E-02	2.46E-04±3.86E-05	<b>2.27E-04±1.70E-05</b>	2.37E-04±1.84E-05	2.35E-04±1.79E-05	2.34E-04±2.41E-05	1.64E-02±8.80E-02	
		Energy	4.18E+00±1.31E-01	2.52E+02±3.54E-02	1.96E+02±7.49E-01	1.31E+02±3.80E+01	2.56E+00±4.65E-02	2.44E+00±8.20E-03	<b>2.43E+00±8.12E-03</b>	2.43E+00±7.97E-03	2.44E+00±9.18E-03	3.05E+00±3.70E-01	
	0.001	S1	RunTime	2.41E+02±2.76E+01	2.69E+02±2.11E+01	<b>8.02E+01±1.68E-01</b>	8.34E+01±6.29E+00	2.68E+02±2.29E+01	5.37E+02±3.44E+01	2.50E+02±6.41E+01	2.25E+02±6.52E+01	2.25E+02±2.11E+01	2.44E+02±1.21E+01
			Fidelity	9.12E-01±3.36E-03	<b>9.99E-01±1.81E-04</b>	9.61E-01±2.92E-02	9.64E-01±2.64E-02	9.04E-01±1.71E-02	8.93E-01±2.92E-02	9.14E-01±4.39E-04	9.14E-01±1.82E-04	9.13E-01±6.76E-03	4.66E-01±2.16E-01
			Deviation	2.57E-02±9.70E-04	<b>3.17E-04±4.24E-05</b>	1.44E-02±1.48E-02	1.04E-02±6.94E-03	2.77E-02±4.54E-03	3.13E-02±7.68E-03	2.47E-02±4.39E-05	2.47E-02±2.25E-05	2.51E-02±1.72E-03	2.27E-01±1.21E-01
S2		Energy	4.29E+00±4.19E-02	3.77E+00±9.55E-03	1.96E+02±5.99E+01	1.27E+02±3.84E+01	4.27E+00±1.42E-01	4.13E+00±7.27E-02	4.17E+00±1.04E-02	4.17E+00±1.04E-02	4.18E+00±4.17E-02	<b>2.71E+00±6.48E-01</b>	
		RunTime	3.03E+02±3.64E+01	3.25E+02±3.46E+01	<b>9.72E+01±4.52E-01</b>	9.95E+01±4.37E+00	3.30E+02±4.21E+01	6.50E+02±4.30E+01	2.88E+02±1.57E+01	2.83E+02±2.31E+00	2.82E+02±7.88E+00	1.21E+02±2.17E+01	
		Fidelity	9.20E-01±4.48E-02	9.48E-01±4.44E-02	9.71E-01±3.63E-02	<b>9.85E-01±1.84E-02</b>	9.68E-01±1.47E-02	9.68E-01±1.13E-02	9.69E-01±1.15E-02	9.69E-01±1.84E-03	9.64E-01±8.75E-03	7.35E-01±2.15E-01	
S3		Deviation	5.40E-02±2.36E-02	3.13E-02±2.36E-02	2.32E-02±3.13E-02	<b>9.94E-03±1.11E-02</b>	1.27E-02±7.76E-03	1.67E-02±5.88E-03	1.61E-02±5.51E-03	1.58E-02±4.09E-03	1.95E-02±5.08E-03	5.44E-01±2.71E-01	
		Energy	7.05E+01±3.36E+00	5.70E+01±4.33E+00	3.08E+02±7.28E+01	2.29E+02±5.77E+01	4.67E+01±5.71E+00	4.31E+01±6.08E+00	3.48E+01±8.41E+00	<b>3.12E+01±8.69E+00</b>	3.42E+01±6.09E+00	6.53E+01±6.92E+00	
		RunTime	2.01E+02±6.27E+00	2.82E+02±1.77E+01	6.71E+01±1.09E+00	<b>6.67E+01±1.09E+00</b>	1.99E+02±2.60E+00	3.91E+02±1.79E+01	1.88E+02±1.75E+00	1.86E+02±2.31E+00	1.85E+02±1.38E+00	9.49E+01±1.34E+01	
0.0001		S1	Fidelity	9.99E-01±8.40E-04	9.98E-01±1.49E-03	9.69E-01±8.16E-02	9.90E-01±1.21E-02	<b>1.00E+00±7.21E-06</b>	<b>1.00E+00±5.72E-06</b>	<b>1.00E+00±5.84E-06</b>	<b>1.00E+00±7.03E-06</b>	1.00E+00±8.79E-05	9.67E-01±1.74E-01
			Deviation	3.77E-04±2.28E-04	6.46E-04±3.91E-04	1.02E-02±2.57E-02	3.64E-03±3.88E-03	4.07E-06±1.99E-06	3.55E-06±1.75E-06	<b>3.32E-06±1.45E-06</b>	3.42E-06±1.78E-06	3.52E-05±2.57E-05	1.34E-02±7.11E-02
			Energy	5.21E+00±2.43E-01	6.10E+00±4.91E-01	7.26E+02±7.26E+01	6.55E+02±7.46E+01	2.93E+00±1.03E-01	2.68E+00±7.56E-02	2.67E+00±6.70E-02	<b>2.67E+00±4.71E-02</b>	3.32E+00±1.28E-01	3.24E+00±4.19E-01
	S2	RunTime	1.81E+02±8.24E+00	1.85E+02±4.32E-01	5.99E+01±2.20E-01	<b>5.98E+01±2.60E-01</b>	1.77E+02±3.33E-01	3.52E+02±5.35E-01	1.79E+02±3.99E-01	1.79E+02±5.23E-01	1.79E+02±9.63E-01	5.85E-01±6.57E+00	
		Fidelity	9.14E-01±4.13E-03	<b>1.00E+00±5.29E-04</b>	9.87E-01±2.18E-02	9.86E-01±2.30E-02	9.03E-01±3.84E-02	8.95E-01±1.94E-02	9.15E-01±3.21E-03	9.15E-01±3.17E-03	9.12E-01±4.99E-03	4.20E-01±2.53E-01	
		Deviation	2.45E-02±1.12E-03	<b>1.37E-04±1.52E-04</b>	1.17E-02±4.05E-02	3.68E-03±5.92E-03	2.74E-02±1.02E-02	3.04E-02±4.99E-03	2.41E-02±8.61E-04	2.41E-02±8.52E-04	2.49E-02±2.54E-03	2.51E-01±1.42E-01	
	S3	Energy	4.62E+00±4.79E-02	5.50E+00±3.81E-01	4.21E+02±3.51E+01	4.00E+02±4.14E+01	4.64E+00±6.75E-02	4.35E+00±5.20E-02	4.58E+00±3.04E-02	4.57E+00±2.29E-02	4.60E+00±5.70E-02	<b>2.60E+00±7.31E-01</b>	
		RunTime	1.86E+02±1.01E+00	1.97E+02±2.19E+00	6.13E+01±2.52E-01	<b>6.13E+01±3.08E-01</b>	1.88E+02±1.92E+00	3.71E+02±6.45E-01	1.89E+02±3.56E-01	1.88E+02±4.57E-01	1.87E+02±1.39E+00	7.81E+01±1.72E-01	
		Fidelity	9.82E-01±1.10E-02	9.72E-01±2.01E-02	9.56E-01±6.54E-02	9.54E-01±8.67E-02	9.88E-01±7.23E-03	9.91E-01±7.22E-03	<b>9.93E-01±4.99E-03</b>	9.92E-01±4.49E-03	9.91E-01±5.36E-03	9.06E-01±6.35E-02	
	0.00001	S1	Deviation	1.14E-02±6.57E-03	1.64E-02±1.14E-02	2.42E-02±3.27E-02	2.36E-02±4.33E-02	6.54E-03±3.55E-03	4.64E-03±3.59E-03	<b>3.35E-03±2.49E-03</b>	4.03E-03±2.28E-03	5.73E-03±2.83E-03	4.33E-01±2.95E-01
			Energy	1.08E+02±8.09E+00	1.57E+02±1.72E+01	7.27E+02±1.06E+02	7.25E+02±8.05E+01	9.57E+01±6.33E+00	8.71E+01±5.18E+00	8.67E+01±5.16E+00	<b>8.67E+01±5.39E+00</b>	9.05E+01±4.82E+00	9.40E+01±3.62E+00
			RunTime	2.74E+02±2.01E+00	2.95E+02±1.70E+00	9.27E+01±2.46E-01	<b>9.25E+01±4.02E-01</b>	2.71E+02±4.22E-01	5.43E+02±2.67E+00	2.75E+02±3.75E+00	2.68E+02±4.89E-01	2.	

### 5.3 Experiments on Multi-objective Physics-informed Evolution

We evaluate the multi-objective PIE framework by comparing five representative multi-objective evolutionary algorithms (NSGA-II, NSGA-III, MOEA/D, SPEA2, and PESA2) across the three quantum control scenarios. For each algorithm, we perform 30 independent runs, and from the obtained Pareto front in each run, we select the solution with the lowest Deviation as the preferred solution. This selection strategy reflects the practical preference in quantum control applications where state accuracy is typically the primary concern, while energy efficiency serves as a secondary consideration. Table 3 reports the mean and standard deviation of Fidelity, Deviation, Energy, and RunTime for the preferred solutions across all runs.

Figure 2 illustrates the experimental results of quantum control in the multi-objective Physics-informed Evolution framework across the three problems. It visualizes the evolution of the physical field  $u$  and the quantum state  $\psi$ , demonstrating the dynamic behavior of the optimal control inputs and the corresponding state responses for the preferred solutions selected from the Pareto front.

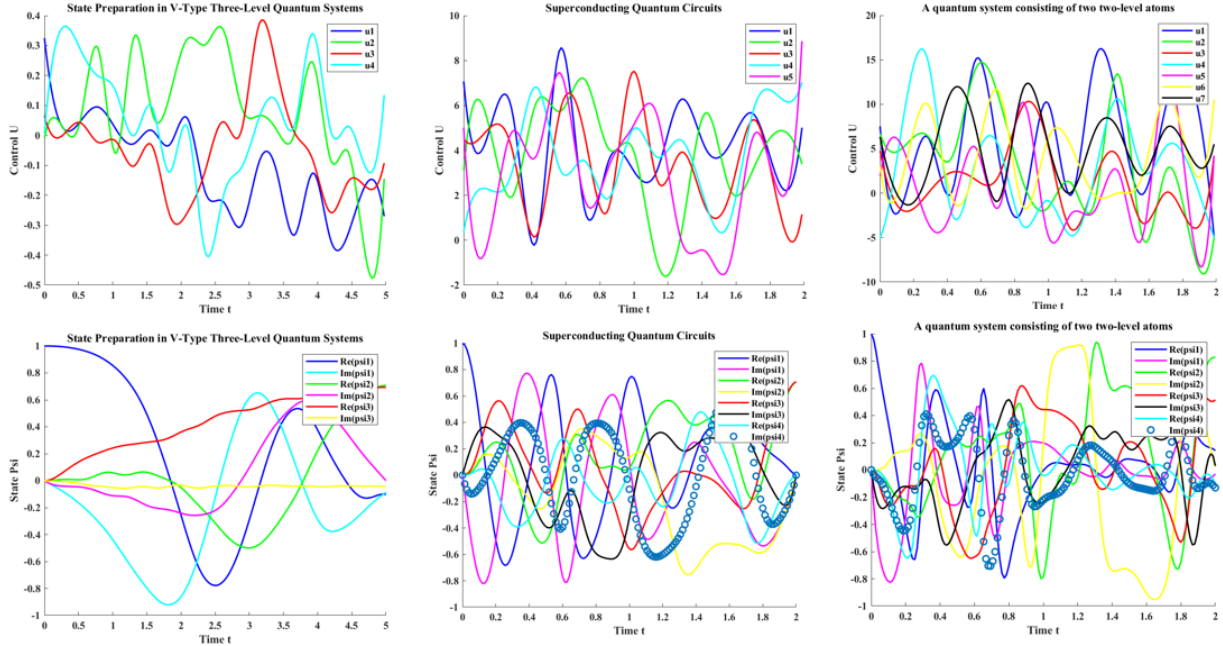


Figure 2: Evolution of control inputs  $u$  and quantum state  $\psi$  for three quantum control problems (S1, S2, S3) in the Multi-Objective Physics-informed Evolution framework. The results correspond to the preferred solutions with the lowest Deviation selected from the obtained Pareto front.

**Scenario S1 (V-type Three-Level System).** In this scenario, PESA2 demonstrates superior performance in terms of state accuracy, achieving the highest fidelity ( $9.89 \times 10^{-1}$ ) and the lowest deviation ( $2.82 \times 10^{-3}$ ) with relatively small standard deviations, indicating

consistent convergence to high-quality solutions. NSGA-II achieves the lowest energy consumption (2.10), making it the most energy-efficient choice, though this comes at the cost of significantly higher deviation ( $3.74 \times 10^{-2}$ ) and lower fidelity. NSGA-III, MOEA/D, and SPEA2 achieve intermediate performance, with SPEA2 showing the second-best deviation ( $1.25 \times 10^{-2}$ ) while maintaining moderate energy consumption (2.76). Regarding runtime, PESA2 is the fastest ( $1.30 \times 10^2$ ), followed by SPEA2 ( $1.44 \times 10^2$ ) and NSGA-III ( $1.48 \times 10^2$ ). The results reveal a clear trade-off: algorithms that prioritize state accuracy (PESA2) consume more energy, while energy-efficient algorithms (NSGA-II) sacrifice fidelity.

**Scenario S2 (Superconducting Quantum Circuits).** NSGA-II achieves exceptional performance in this scenario, obtaining perfect fidelity (1.00) and the lowest deviation ( $5.47 \times 10^{-6}$ ) with extremely small standard deviations, demonstrating remarkable consistency and effectiveness for this particular quantum control problem. NSGA-III follows closely with near-perfect fidelity ( $9.99 \times 10^{-1}$ ) and low deviation ( $1.44 \times 10^{-4}$ ), while achieving the lowest energy consumption ( $3.23 \times 10^1$ ) among all algorithms—slightly better than NSGA-II’s  $3.32 \times 10^1$ . MOEA/D, SPEA2, and PESA2 show progressively degraded performance, with fidelity decreasing to  $7.95 \times 10^{-1}$  for PESA2 and deviation increasing to  $6.18 \times 10^{-2}$ . This dramatic performance gap suggests that the Pareto front structure in S2 may favor algorithms with specific selection mechanisms. PESA2 again provides the fastest runtime ( $1.38 \times 10^2$ ), while NSGA-II is the slowest ( $1.74 \times 10^2$ ). Notably, NSGA-II and NSGA-III demonstrate that high fidelity and reasonable energy efficiency can be simultaneously achieved in this scenario.

**Scenario S3 (Two-Atom Cavity QED System).** MOEA/D achieves the best state accuracy in this mixed-state scenario, with the highest fidelity ( $9.64 \times 10^{-1}$ ) and lowest deviation ( $1.79 \times 10^{-2}$ ), outperforming all other algorithms. SPEA2 achieves the lowest energy consumption ( $6.43 \times 10^1$ ) while maintaining moderate fidelity ( $9.27 \times 10^{-1}$ ), representing an alternative trade-off point on the Pareto front. NSGA-II and NSGA-III show similar intermediate performance, with fidelity around  $9.40 \times 10^{-1}$  and deviation around  $3.00 \times 10^{-2}$ , while consuming slightly more energy than SPEA2 ( $7.39 \times 10^1$  and  $7.04 \times 10^1$  respectively). PESA2 again provides the fastest runtime ( $2.01 \times 10^2$ ), followed by SPEA2 ( $2.10 \times 10^2$ ) and MOEA/D ( $2.15 \times 10^2$ ). The results demonstrate that different algorithms capture different regions of the Pareto front: MOEA/D focuses on the high-fidelity region, while SPEA2 explores the energy-efficient region.

**Overall Observations.** Several important patterns emerge from the multi-objective comparison. First, no single algorithm dominates across all scenarios, highlighting the importance of algorithm selection based on the specific quantum control problem characteristics. PESA2 excels in S1, NSGA-II dominates S2, and MOEA/D leads in S3 when state accuracy is prioritized. Second, the trade-off between Deviation and Energy is clearly manifested: algorithms achieving the lowest deviation (PESA2 in S1, NSGA-II in S2, MOEA/D in S3) generally consume more energy than the most energy-efficient alternatives, confirming the competing nature of these two objectives. Third, runtime performance is relatively

consistent, with PESA2 being the fastest across all scenarios and NSGA-II generally the slowest, reflecting the computational overhead of their respective selection mechanisms. Finally, the multi-objective PIE framework successfully generates diverse Pareto-optimal solutions, and our preference-based selection strategy (choosing the lowest-deviation solution) effectively identifies control strategies that prioritize state accuracy while still benefiting from the multi-objective optimization process that explicitly considers the energy trade-off.

Table 3: Multi-objective

Sence	Metrics	NSGA-II	NSGA-III	MOEA/D	SPEA2	PESA2
S1	Fidelity	8.58E-01±8.29E-02	9.32E-01±5.00E-02	9.27E-01±3.07E-02	9.52E-01±3.33E-02	<b>9.89E-01±4.23E-03</b>
	Deviation	3.74E-02±2.23E-02	1.76E-02±1.30E-02	2.10E-02±9.59E-03	1.25E-02±8.62E-03	<b>2.82E-03±1.12E-03</b>
	Energy	<b>2.10E+00±2.34E-01</b>	2.25E+00±1.71E-01	3.00E+00±2.26E-01	2.76E+00±3.29E-01	3.10E+00±1.30E-01
	RunTime	1.60E+02±4.08E+00	1.48E+02±6.52E-01	1.50E+02±1.38E+01	1.44E+02±1.35E+00	<b>1.30E+02±2.32E+00</b>
S2	Fidelity	<b>1.00E+00±1.49E-05</b>	9.99E-01±1.22E-03	9.53E-01±3.76E-02	8.47E-01±1.61E-01	7.95E-01±9.41E-02
	Deviation	<b>5.47E-06±3.66E-06</b>	1.44E-04±3.04E-04	2.14E-02±2.90E-02	4.35E-02±4.57E-02	6.18E-02±2.78E-02
	Energy	3.32E+01±2.68E+00	<b>3.23E+01±1.61E+00</b>	4.52E+01±7.87E+00	3.29E+01±7.15E+00	3.49E+01±5.12E+00
	RunTime	1.74E+02±1.26E+00	1.64E+02±8.70E-01	1.42E+02±4.12E+00	1.45E+02±4.73E-01	<b>1.38E+02±7.74E-01</b>
S3	Fidelity	9.40E-01±4.32E-02	9.39E-01±3.33E-02	<b>9.64E-01±2.15E-02</b>	9.27E-01±2.36E-02	9.29E-01±3.51E-02
	Deviation	3.00E-02±2.16E-02	3.06E-02±1.66E-02	<b>1.79E-02±1.09E-02</b>	3.86E-02±1.26E-02	4.15E-02±1.88E-02
	Energy	7.39E+01±1.25E+01	7.04E+01±1.18E+01	9.21E+01±3.78E+00	<b>6.43E+01±7.36E+00</b>	7.44E+01±5.92E+00
	RunTime	2.43E+02±4.56E+00	2.32E+02±8.35E-01	2.15E+02±1.98E+00	2.10E+02±7.31E-01	<b>2.01E+02±2.53E+00</b>

## 6 Conclusions and Future Work

In this paper, we have introduced Physics-Informed Evolution (PIE), a novel framework that embeds physical information derived from governing physical laws into the fitness function of evolutionary algorithms. Drawing a direct and principled analogy with Physics-Informed Neural Networks (PINNs), we have demonstrated that the same physical insight that guides gradient-based learning can also shape evolutionary search. By incorporating energy consumption as a physics-informed regularization term (in the single-objective formulation) or as a competing objective (in the multi-objective formulation), PIE guides evolutionary algorithms toward solutions that are not only high-performing in terms of task objectives but also physically meaningful and efficient.

We have validated the PIE framework on three challenging quantum control problems governed by the Schrödinger equation: state preparation in V-type three-level systems, entangled state generation in superconducting quantum circuits, and control of two-atom cavity QED systems. Through extensive experiments under various regularization parameter settings, we have compared ten single-objective and five multi-objective evolutionary baselines. The results consistently demonstrate that adaptive differential evolution variants (JADE, CJADE, SHADE) achieve the highest fidelity and lowest deviation within the PIE framework, while CMA-ES shows remarkable robustness in specific scenarios. The trade-off controlled by the regularization parameter  $\lambda$  is clearly evident: larger  $\lambda$  yields more energy-efficient solutions at the cost of increased state deviation, validating the framework’s ability

to generate a spectrum of solutions from high-fidelity to energy-efficient control strategies. In the multi-objective setting, our preference-based selection strategy effectively identifies control strategies that prioritize state accuracy while benefiting from explicit consideration of the energy trade-off, with different algorithms excelling in different scenarios.

Beyond empirical validation, this work establishes a broader conceptual bridge between the physics-informed learning paradigm and evolutionary computation. The success of PIE suggests that the principle of embedding physical information into optimization objectives extends naturally beyond gradient-based neural network training to derivative-free, population-based search.

Several promising directions emerge from this research. First, the deep connection between learning and evolution deserves further exploration within the physics-informed context—investigating how individual learning and population-level evolution can mutually reinforce each other in pursuing physically consistent solutions. Second, developing differentiable evolutionary frameworks could enable backpropagation through the entire evolutionary process, allowing physical information to guide not only fitness evaluation but also evolutionary dynamics. Third, extending PIE to incorporate physical principles directly into evolutionary operators—such as mutation respecting physical symmetries or crossover preserving physically meaningful structures—could further enhance solution quality. Finally, while this work focuses on quantum control, the PIE framework is general and applicable to any domain governed by physical laws, including classical mechanics, fluid dynamics, electromagnetics, and chemical process control, where governing equations can provide physical information to shape evolutionary search.

## References

- [1] Maziar Raissi, Paris Perdikaris, and George E Karniadakis. Physics-informed neural networks: A deep learning framework for solving forward and inverse problems involving nonlinear partial differential equations. *Journal of Computational physics*, 378:686–707, 2019.
- [2] George Em Karniadakis, Ioannis G Kevrekidis, Lu Lu, Paris Perdikaris, Sifan Wang, and Liu Yang. Physics-informed machine learning. *Nature Reviews Physics*, 3(6):422–440, 2021.
- [3] Xingyu Wu, Sheng-hao Wu, Jibin Wu, Liang Feng, and Kay Chen Tan. Evolutionary computation in the era of large language model: Survey and roadmap. *IEEE Transactions on Evolutionary Computation*, 29(2):534–554, 2024.
- [4] Anton V Sinitskiy. Making sense of neural networks in the light of evolutionary optimization. *bioRxiv*, pages 2023–11, 2023.

- [5] Stephen Whitelam, Viktor Selin, Sang-Won Park, and Isaac Tamblyn. Correspondence between neuroevolution and gradient descent. *Nature communications*, 12(1):6317, 2021.
- [6] Kaichen Ouyang, Zong Ke, Shengwei Fu, Lingjie Liu, Puning Zhao, and Dayu Hu. Learn from global correlations: Enhancing evolutionary algorithm via spectral gnn. *arXiv preprint arXiv:2412.17629*, 2024.
- [7] Kaichen Ouyang, Shengwei Fu, Yi Chen, and Huiling Chen. Dynamic graph neural evolution: An evolutionary framework integrating graph neural networks with adaptive filtering. In *2025 IEEE Congress on Evolutionary Computation (CEC)*, pages 1–8. IEEE, 2025.
- [8] Kaichen Ouyang, Mingyang Yu, Zong Ke, Junbo Jacob Lian, Shengwei Fu, Xiaoyang Hao, Shengju Yu, and Dayu Hu. Wasserstein evolution: Evolutionary optimization as phase transition. *arXiv preprint arXiv:2512.05837*, 2025.
- [9] Daoyi Dong, Mohamed A Mabrok, Ian R Petersen, Bo Qi, Chunlin Chen, and Herschel Rabitz. Sampling-based learning control for quantum systems with uncertainties. *IEEE Transactions on Control Systems Technology*, 23(6):2155–2166, 2015.
- [10] Rainer Storn and Kenneth Price. Differential evolution—a simple and efficient heuristic for global optimization over continuous spaces. *Journal of global optimization*, 11(4):341–359, 1997.
- [11] Nikolaus Hansen, Sibylle D Müller, and Petros Koumoutsakos. Reducing the time complexity of the derandomized evolution strategy with covariance matrix adaptation (cma-es). *Evolutionary computation*, 11(1):1–18, 2003.
- [12] Xiaoyu He, Zibin Zheng, and Yuren Zhou. Mmes: Mixture model-based evolution strategy for large-scale optimization. *IEEE Transactions on Evolutionary Computation*, 25(2):320–333, 2020.
- [13] Xiaoyu He, Yuren Zhou, Zefeng Chen, Jun Zhang, and Wei-Neng Chen. Large-scale evolution strategy based on search direction adaptation. *IEEE Transactions on Cybernetics*, 51(3):1651–1665, 2019.
- [14] A Kai Qin and Ponnuthurai N Suganthan. Self-adaptive differential evolution algorithm for numerical optimization. In *2005 IEEE congress on evolutionary computation*, volume 2, pages 1785–1791. IEEE, 2005.
- [15] Jingqiao Zhang and Arthur C Sanderson. Jade: adaptive differential evolution with optional external archive. *IEEE Transactions on evolutionary computation*, 13(5):945–958, 2009.

- [16] Shangce Gao, Yang Yu, Yirui Wang, Jiahai Wang, Jiujun Cheng, and MengChu Zhou. Chaotic local search-based differential evolution algorithms for optimization. *IEEE Transactions on Systems, Man, and Cybernetics: Systems*, 51(6):3954–3967, 2019.
- [17] Ryoji Tanabe and Alex Fukunaga. Success-history based parameter adaptation for differential evolution. In *2013 IEEE congress on evolutionary computation*, pages 71–78. IEEE, 2013.
- [18] Ryoji Tanabe and Alex S Fukunaga. Improving the search performance of shade using linear population size reduction. In *2014 IEEE congress on evolutionary computation (CEC)*, pages 1658–1665. IEEE, 2014.
- [19] Petr Bujok and Patrik Kolenovsky. Eigen crossover in cooperative model of evolutionary algorithms applied to cec 2022 single objective numerical optimisation. In *2022 IEEE congress on evolutionary computation (CEC)*, pages 1–8. IEEE, 2022.
- [20] Kalyanmoy Deb, Amrit Pratap, Sameer Agarwal, and TAMT Meyarivan. A fast and elitist multiobjective genetic algorithm: Nsga-ii. *IEEE transactions on evolutionary computation*, 6(2):182–197, 2002.
- [21] Kalyanmoy Deb and Himanshu Jain. An evolutionary many-objective optimization algorithm using reference-point-based nondominated sorting approach, part i: solving problems with box constraints. *IEEE transactions on evolutionary computation*, 18(4):577–601, 2013.
- [22] Qingfu Zhang and Hui Li. Moea/d: A multiobjective evolutionary algorithm based on decomposition. *IEEE Transactions on evolutionary computation*, 11(6):712–731, 2007.
- [23] Eckart Zitzler, Marco Laumanns, and Lothar Thiele. Spea2: Improving the strength pareto evolutionary algorithm. *TIK report*, 103, 2001.
- [24] David W Corne, Joshua D Knowles, and Martin J Oates. The pareto envelope-based selection algorithm for multiobjective optimization. In *International conference on parallel problem solving from nature*, pages 839–848. Springer, 2000.
- [25] Selection Algorithm II. Ipesa-ii: Improved pareto envelope-based. In *Evolutionary Multi-Criterion Optimization: 7th International Conference, EMO 2013, Sheffield, UK, March 19-22, 2013. Proceedings*, page 143. Springer, 2013.